Kinetics of Oriented Aggregation

R. Lee Penn*

Department of Chemistry, University of Minnesota, 207 Pleasant Street SE, Minneapolis, Minnesota 55455

Received: August 21, 2003; In Final Form: June 11, 2004

Oriented aggregation is a special case of aggregation that provides an important route by which nanocrystals grow, defects are formed, and unique, often symmetry-defying, crystal morphologies are produced. This growth mechanism involves the irreversible and crystallographically specific self-assembly of primary nanocrystals and results in the formation of new single crystals, twins, and intergrowths. This paper presents a molecular model for the mechanism of oriented aggregation. This model involves a rapid equilibrium for the association and dissociation of nanocrystals and an irreversible conversion of associated nanocrystals for producing oriented aggregates.

Oxide, oxyhydroxide, hydroxide, selenide, and sulfide nanoparticles are commonly synthesized from homogeneous solutions[1−4] and are extensively used in energy conversion, optical coatings, catalysis, and other applications. Furthermore, nanoparticles are ubiquitous on and near the Earth's surface, and many of these particles are formed by precipitation from aqueous solutions. Solution-phase methods have become widely used for nanoparticle synthesis and provide models for understanding the precipitation and growth of nanoparticles in the environment. Typically, these methods produce nanoparticles by precipitation from homogeneous solutions.[2−6] This approach has been used for synthesizing semiconductor nanoparticles of II−VI compounds (e.g., CdS,[7,8] CdSe,[7] ZnS,[8] and PbS[9]), III−V compounds (e.g., InAs[7] and GaAs[10]), metal oxides (e.g., ZrO_2,[11] TiO_2,[12,13] ZnO,[14,15] Fe_2O_3,[16,17] and Fe_3O_4[18]), and metal oxyhydroxides (e.g., CoOOH,[6] β-$Co(OH)_2$,[19] feroxyhite,[6] goethite,[20] and manganese hydrous oxides[21−23]).

The size, shape, and microstructure of nanocrystalline materials strongly impact a material's properties and reactivity. Thus, a fundamental understanding of the mechanisms of nanocrystal formation and growth is critical for achieving control over nanoparticle properties. Nanocrystal growth in solution typically involves the fast nucleation of primary particles followed by the subsequent growth by two primary mechanisms: coarsening and aggregation (Figure 1). Coarsening, also known as Ostwald ripening, is a mechanism driven by the fact that the chemical potential of a particle increases with a decrease in particle size, which is described by the Gibbs−Thompson equation. The work of Lifshitz, Slyozov, and Wagner[24,25] derived a rate law for this process by combining the Gibbs−Thompson equation and Fick's first law:

$$\bar{r}^3 - \bar{r}_o^{\,3} = kt \qquad (1)$$

where $\bar{r}$ is the average particle size at time t, $\bar{r}_o$ is the average initial particle size, and k is the rate constant. This rate law is commonly used for describing diffusion-limited particle growth in solid states and in liquids. Thus, larger particles grow at the expense of smaller particles by the diffusion of molecular-scale species through solution.[1,26] An ideal synthesis produces monodisperse particles which are often defined as having a standard deviation in diameter of <5%.[1] Previous work has shown that nucleation must occur over an extremely short time period and be followed by slow, controlled growth by diffusion of molecular-scale species to the surfaces of existing nuclei in order to produce a monodispersed sample of particles.[1,27] In addition, recent work has shown that Ostwald ripening does not adequately describe the kinetics of particle growth for many systems.[28,29]

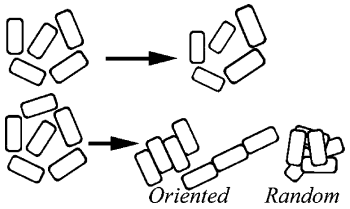

Figure 1. Schematic illustrating end-member nanocrystal growth mechanisms: (top) coarsening, which involves the growth by diffusion of molecular-scale species from smaller crystals to larger crystals, and (bottom) growth by aggregation.

At the other end of the spectrum, the controlled synthesis of monodispersed and polycrystalline colloidal particles often involves the nucleation of primary particles followed by their aggregation. The kinetic models describing growth by aggregation often use formulations that are similar to the Smoluchowski model of colloidal growth.[28,30−33] The particles formed in this manner are commonly polycrystalline particles that are composed of randomly oriented primary nanocrystallites.[32,34] In some cases, the secondary particles exhibit regions with a substantial preferred orientation of the primary nanocrystallites. In extreme cases, the secondary particles are new single crystals composed of oriented subunits.[29,35−37] This commonly overlooked and understudied nanoparticle growth mechanism is oriented aggregation, a special case of aggregation whereby primary particles attach to one another in an irreversible and highly oriented fashion to produce secondary particles that are new single crystals or pseudocrystals (Figure 2). Growth is accomplished by the removal of solvent and/or adsorbed molecules and the formation of chemical bonds at the interface between primary particles. The total energy is decreased as a result of the elimination of the solid−liquid or solid−gas interface[38] and

* penn@chem.umn.edu.

10.1021/jp036490+ CCC: $27.50
Published on Web 07/29/2004

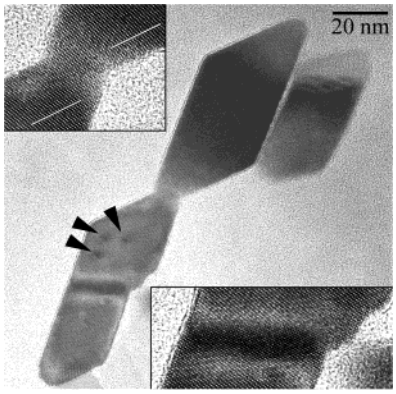

Figure 2. HRTEM image of an anatase (TiO_2) nanocrystal formed by oriented aggregation and coarsening. The insets are higher-magnification images of the interfaces between primary building blocks. The original interface, which is magnified in the upper left-hand inset, is still visible. The white lines in the upper left-hand inset highlight the slight misorientation between the upper and lower region of the crystal. The black arrowheads highlight three of several dislocations in this crystal. This sample was prepared by sol−gel synthesis followed by hydrothermal aging at 250 °C, as described by Penn and Banfield (ref 38). This image was taken using an FEI CM200.

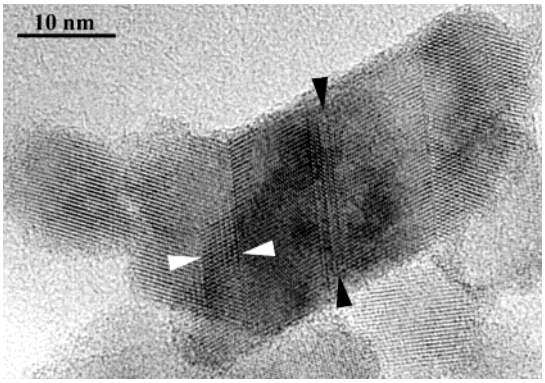

Figure 3. HRTEM image of an anatase (TiO_2) nanocrystal formed by oriented aggregation and coarsening. The white arrowheads highlight a slab of material that is inferred to be an eight- or nine-layer wide nucleus of rutile (see Penn and Banfield, ref 41). The black arrowheads highlight a three-unit cell wide strip of brookite (see Penn and Banfield, ref 39). This sample was prepared by sol−gel synthesis followed by hydrothermal aging at 250 °C, as described by Penn and Banfield (refs 38, 39, and 41). This image was taken using an FEI CM200.

an increase in entropy. When primary particle surfaces contain steps, oriented aggregation across those surfaces can produce edge and screw dislocations (Figure 3).[38] Since oriented aggregation only requires a two-dimensional structural accord within the plane of the approaching surfaces, twins, stacking faults, and intergrowths can form (Figure 3).[39] In addition, new atomic-scale structural units formed at the interface (e.g., a twin or stacking fault) between two primary nanoparticles may serve as nuclei for subsequent phase transformations.[40,41]

To determine whether an individual particle has formed by oriented aggregation or by another complex growth mechanism, high-resolution imaging is required. To date, high-resolution transmission electron microscopy (HRTEM) has been the only technique that can resolve the subnanometer length-scale features that demonstrate aggregation-based nanoparticle growth. Micrographs are examined for variations in contrast, dimpled boundaries, lattice fringe clarity, and alignment across the breadth of a particle, and for the presence of defects such as edge and screw dislocations. Additional information can be obtained by tilting the particle to a second orientation using a double-tilt TEM holder. In particles formed by Ostwald ripening, features such as dimples and defects (except point defects) are expected to be absent. Furthermore, the recrystallization of randomly oriented primary particles is expected to ultimately remove structural features such as edge dislocations and dimpled boundaries.[42] A major challenge in this image-based evaluation is that recrystallized oriented aggregates and particles formed by simultaneous coarsening and oriented aggregation may not exhibit the features that are characteristic of oriented and misoriented aggregation. Furthermore, such work is extremely time consuming. However, examining a subset of electron micrographs published in the last several years reveals that evidence for oriented aggregation is quite common for a range of synthetic conditions. Alternative nanoparticle synthesis methods in which evidence for oriented attachment has been observed include laser ablation of precursors (e.g., ZrO_2[43] and CeO_2[44]), heat treatment of amorphous nanoparticles in air (TiO_2[45]), and plasma synthesis methods (TiC[46]). Furthermore, recent work has highlighted the importance of oriented aggregation in the formation of natural nanoparticles.[47,48] Table 1 lists some examples of recent work in which evidence for oriented aggregation is observed in the published electron micrographs of synthetic materials.

Kinetic modeling of particle growth yields critical information regarding particle growth mechanisms. Huang et al. recently published a kinetic model involving two-stage growth for ZnS nanoparticles in aqueous suspensions containing mercaptoethanol as a passivating agent. The first stage of growth was inconsistent with the kinetics of Ostwald ripening, and their HRTEM images suggested that oriented aggregation was clearly occurring. Thus, they developed a model of growth by oriented aggregation. They defined this model in terms of the number of particles consisting of a single primary particle and the number of particles consisting of two primary particles. Furthermore, they described their kinetic model for oriented aggregation in terms of the volume-weighted average particle size so that they could use the particle size data collected using X-ray diffraction line-broadening analysis. The first stage of particle growth was fit well using their model, and the second stage of growth was fit well using the accepted kinetic model for Ostwald ripening.[28]

This paper's focus is the development of a kinetic model for oriented aggregation. Suppose that primary nanoparticles can be viewed as molecules, as discussed by Penn and Banfield.[38] The first of two simple possibilities is that two primary particles collide to irreversibly produce an oriented aggregate only if their orientation at the time of collision achieves two-dimensional structural accord at the interface (eq 2). If the particles collide without a compatible orientation, then no reaction occurs. P represents a primary particle, and the line represents the chemical bonds between two oriented primary particles (i.e., conversion to a new single crystal, twin, or intergrowth).

$$\mathrm{P} + \mathrm{P} \xrightarrow[-x\mathrm{H_2O}]{k} \mathrm{P{-}P} \qquad (2)$$

The second possibility is that two primary particles collide to produce a "complex", denoted by P···P, that can subsequently

TABLE 1: Examples of Oriented Aggregation[a]

first author	year	ref	material	microstructure/morphology	estimated no. of primary particles
Penn	1999	41	TiO_2	rutile elbows and anatase twins	>2
Penn	1999	39	TiO_2	anatase twins	>2
				anatase, brookite intergrowths	>2
				varied anatase morphologies	>2
Penn	1998	38	TiO_2	varied anatase morphologies	>2
Scolan	1998	59	TiO_2	oriented aggregates	>3
Chemseddine	1999	60	TiO_2	elongated and corrugated	tens
Shen	2001	43	ZrO_2	coalescence twins	2
Lou	2003	61	MoO_3, TiO_2	TiO_2 horseshoes	several
Lee	1999	62	CeO_2	twins and octahedra attached across {100}	2
Pacholski	2002	63	ZnO	nanorods	>2
Cozzoli	2003	64	ZnO	elongated particles	>2
Niederberger	2002	65	hematite (Fe_2O_3)	rounded hexagonal plates	hundreds
Penn	2001	42	Fe_2O_3	rounded hematite particles	tens
			FeOOH	irregular feroxyhite plates	hundreds
			CoOOH	hexagonal plates	hundreds
			anatase	varied	>2
Guyodo	2003	66	α-FeOOH	goethite nanorods	several
Nesterova	2003	67	FeOOH	various	>2
Zhang	2000	68	sulfides, oxides	prisms, spindles, needles	>2
Audinet	1999	69	core−shell CdS/ZnS	rounded particles with dimples and defects	several
Banfield	2001	48	ZnS	twins, stacking faults, intergrowths	several
Huang	2003	28	ZnS	irregular-shaped oriented aggregates	several
Ricolleau	1999	70	CdS	twins, stacking faults	>2
			CdS−ZnS	rounded and dimpled	several
Sampanthar	2002	19	β-$Co(OH)_2$	"butterflies"	tens to hundreds
Shen	2001	37	MCM-41	mesoporous	hundreds
Nikolakis	2000	71	zeolite	rounded	hundreds
de Moor	1999	72	zeolite (ZDM-5)	rounded	tens
Kuo	2000	46	α-Ti, TiC	rounded aggregate with shared atomic planes	3
Wang	2000	73	Pt	elongated morphology	2

[a] Published within the last five years.

dissociate or react to form an oriented aggregate (eqs 3−5).

$$\mathrm{P} + \mathrm{P} \xrightarrow{k_1} \mathrm{P{\cdots}P} \tag{3}$$

$$\mathrm{P{\cdots}P} \xrightarrow{k_1} \mathrm{P} + \mathrm{P} \tag{4}$$

$$\mathrm{P{\cdots}P} \xrightarrow[-x\mathrm{H_2O}]{k_2} \mathrm{P{-}P} \tag{5}$$

In this case, the requirement that the primary nanoparticles be in compatible orientations does not apply. In other words, complexed primary nanoparticles can be viewed as outer-sphere complexes, and the primary particles would be free to rotate into an orientation that achieves structural accord at the interface. In both models, adsorbed solvent molecules (e.g., hydroxyls, protons, and water molecules in the case of aqueous suspensions) and other species must be irreversibly removed from the interface (denoted $-x\mathrm{H_2O}$ in eqs 2 and 5) or incorporated into the bulk. For example, in an aqueous suspension at a pH near the $\mathrm{pH_{zpc}}$, particle coalescence will involve a simple condensation reaction, yielding water molecules, protons, and/or hydroxyls as the products of removing nonconstituent, surface-bound species and forming bonds between the two approaching surfaces. Furthermore, it has been suggested that the presence of such surface species may facilitate the reorientation of two contacting nanoparticles, which could be driven by Brownian motion.[28]

In the first model, the rate of oriented aggregation will be second-order in the concentration of primary nanoparticles (eq 6).

$$\mathrm{d(P{-}P)/d}t = k(\mathrm{P})^2 \tag{6}$$

In the second model, which is a modified version of the Lindemann−Hinshelwood mechanism, it can be shown that a steady-state assumption for the concentration of P···P complexes yields a rate law that is also second-order in the concentration of primary nanoparticles (eq 7).

$$\mathrm{d(P{-}P)/d}t = k_1k_2(\mathrm{P})^2/(k_{-1} + k_2) \tag{7}$$

Furthermore, it can be shown that a rapid equilibrium assumption for the concentration of P···P complexes (analogous to the Eigen−Wilkins ligand-exchange mechanism) also yields a rate law that is second-order in the concentration of primary nanoparticles (eq 8).

$$\mathrm{d(P{-}P)/d}t = (k_1/k_{-1})k_2(\mathrm{P})^2 \tag{8}$$

In the case of the rapid equilibrium model (eq 8), the stability constant for the particle encounter complex ($K_{OS} = k_{-1}/k_1$) can be estimated using a combination of the DLVO (Derjaguin, Landau, Verwey, and Overbeek) theory and the Fuoss equation. Using the DLVO theory,[49−51] we can calculate the electrostatic and van der Waals contributions to the interaction energy between two particles (eqs 9−11).

$$V_T(h) = \pi R\left(\frac{-H_{121}}{12\pi h} + \frac{64c_{io}^{*}kT\Gamma_o^{\,2}e^{-\kappa h}}{\kappa^2}\right) \tag{9}$$

where for a symmetrical electrolyte (e.g., NaCl)

$$\frac{1}{\kappa} = \frac{\epsilon_r\epsilon_o kT}{2000e^2N_{Av}I} \tag{10}$$

where

$$\Gamma_o = \frac{\exp(ze\Phi_o/2kT) - 1}{\exp(ze\Phi_o/2kT) + 1} \quad (11)$$

and where $V_T(h)$ is the total interaction energy between two spherical particles, R is the radius of the particle (spherical), h is the separation distance between particles (meters), H_{121} is the Hamaker constant for the two particles (1) in a liquid medium (2), c_{io}^* is the bulk concentration of electrolyte (number concentration), ze is the charge on the electrolyte ions (in this case, $1e^+$ and $1e^-$), Φ_o is the surface potential (volts), k is Boltzmann's constant, T is temperature (kelvin), ϵ_r is the unitless dielectric constant of the medium, ϵ_o is the vacuum permittivity, κ is the reciprocal of the Debye length (meters^{-1}), and N_{Av} is Avogadro's number.

Although the above information does not include contributions for hydrogen bonding and other non-DLVO interactions, it serves as a starting point for estimating the stability constant for the encounter complex. Using the Fuoss equation, we can calculate the stability constant for an outer-sphere complex using the electrostatic interaction energy between the two ions, which are modeled as point charges[52]. Combining eq 9 with the Fuoss equation results in eq 12 (written in SI units).

$$K_{OS} = \frac{4000\pi N_{Av} h^3}{3} \exp(-V_T(h)/kT) \quad (12)$$

Using a surface potential of 50 mV, an ionic strength of 0.01 M, a separation distance of 0.5 nm, a Hamaker constant of 5×10^{-20} J (aqueous medium[51]), a temperature of 80 °C (midrange for many oxide nanoparticle synthesis procedures), and a unitless dielectric constant for water at 80 °C (ϵ_r) of 60.86,[53] we obtained a stability constant of 0.3 (approximately one in 100 000 particles complexed at equilibrium for a loading value of approximately 1 g/L and a particle size of approximately 4 nm). As the surface potential increases, the stability constant decreases. This is consistent with experimental results that show that particles grow more slowly by oriented aggregation when the suspension conditions are such that the particles are highly charged (i.e., several pH units away from the pH_{zpc}).[29,38,39,41,54] Using the above approach, a stability constant on the order of 10^{-1} results in an estimated k_2 of $\sim 10^3$ h^{-1} for experiments involving growth of goethite particles from ferrihydrite nanoparticles (using data from ref 54).

The above estimate of K_{OS} assumes a spherical particle shape and a homogeneous distribution of surface charge over the surface of the particle. The pH_{zpc} for the individual crystal faces deviates from the average pH_{zpc} of the entire particle due to the different coordination environments of surface and near-surface atoms at the various crystal surfaces (see, for example, work by Sverjensky and co-workers,[55] by Van Reimjsdik and co-workers,[56] and by Rustad[57]). Thus, the above approach produces a minimum estimate of the stability constant. Furthermore, the largest differences in oriented aggregation are expected when the suspension pH is near the average pH_{zpc} of the crystallite. Near the pH_{zpc}, particles are expected to have some negatively charged surfaces and some positively charged surfaces, in which case long-range, attractive electrostatic forces between oppositely charged surfaces could result in a comparatively large K_{OS}. Short-range forces (i.e., van der Waals forces and hydrogen bonding), Brownian motion, and the increase in entropy resulting from the removal of surface-adsorbed water (or other solvent) molecules and species could then drive the subsequent reorientation and conversion to an oriented aggregate.

The rate laws presented (eqs 6−8) are consistent with the generalized model for oriented aggregation, which is second-order in the number of primary particles, presented by Huang et al.[28] The conversion of these rate laws from the concentration of nanoparticles to the number of nanoparticles is straightforward. Furthermore, the second model (eqs 7 and 8) is consistent with the results of Zhu and Averback, who used molecular dynamics simulations to show that when two copper crystallites are attached in random orientations, the crystallites rotate with respect to one another in order to achieve structural accord at the contact surface.[58] The simulations of Zhu and Averback are analogous to the conversion of a P···P complex to an oriented aggregate without the presence of a solvent and/or other species at the contact surface.

Examination of the data published by Huang et al.[28] and Penn et al.[42] provides the necessary clues for distinguishing between these two basic models. Penn et al. showed that anatase (TiO_2) growth by oriented aggregation slowed with an increase in temperature.[42] In contrast, Huang et al. showed that the rate of oriented aggregation increased with an increase in temperature (below 225 °C for ZnS nanoparticles) and determined an activation energy for oriented attachment by fitting particle size (determined by XRD) results from experiments that were performed at several different temperatures.[28]

In the first model, the rate of oriented aggregation would be expected to increase with an increase in temperature. Thus, it is not consistent with both results. On the other hand, the second model is consistent with both results. In the case of Penn et al., the decreased rate of oriented aggregation with an increase in temperature may indicate that the association−dissociation equilibrium is the dominant step since k_1/k_{-1} is expected to decrease with an increase in temperature. In other words, the activation energy for the conversion of P···P to P−P is small in comparison to the activation energies of association and dissociation. In the case of Huang et al., the increased oriented aggregation with an increase in temperature may indicate that the conversion of associated nanoparticles into oriented aggregates is the dominant step since k_2 is expected to increase with an increase in temperature. If this second model is correct, then the activation energy determined by Huang et al. is $E_a^{association} + E_a^{OA} - E_a^{dissociation}$ (OA denotes conversion to an oriented aggregate).

The inverse temperature dependence observed by Penn et al. most likely indicates that the activation energy for conversion from a complex to an oriented aggregate is substantially smaller than the activation energies for association and dissociation. On the other hand, the positive temperature dependence observed by Huang et al. most likely indicates that the activation energy for conversion from a complex to an oriented aggregate is comparable or substantially larger than the activation energies for association and dissociation. Both studies used aqueous suspensions of particles, but a key difference between the experiments is that Huang et al. used a passivating agent and metal sulfide particles[28] while Penn et al. used no passivating agent and metal oxide particles. In both cases, the passivating agent (if present) and excess water molecules, hydroxyls, and protons must be removed from the interface in order to form an oriented aggregate. While the removal of water molecules from the sulfide surface is likely to require less energy than from the oxide surface, the removal of passivating agents from nanoparticle surfaces is expected to require additional energy. In the context of oriented aggregation, water may act as a

coordinating solvent for oxide surfaces but not for sulfide surfaces. Furthermore, the presence of passivating agents may have substantially altered both the association−dissociation of primary particles and the conversion from a complex to oriented aggregates.

Altering growth conditions by adding ligands and passivating agents or by changing solvents may provide a route by which growth by oriented aggregation can be controlled. Furthermore, the use of passivating agents may provide a route by which attachment-driven phase transformations can be controlled. Finally, these results have important implications regarding the mechanisms of ligand-assisted nanoparticle assembly in biomineralization.

Acknowledgment. The author acknowledges financial support from the National Science Foundation (Grants EAR-9508171 and CAREER-0346385), the National Physical Science Consortium (fellowship to R.L.P. sponsored by Sandia National Laboratories), the Mineralogical Society of America, and the University of Minnesota. Finally, the author thanks the reviewer for insightful comments.

References and Notes

(1) Murray, C. B.; Kagan, C. R.; Bawendi, M. G. Synthesis and characterization of monodisperse nanocrystals and close-packed nanocrystal assemblies. *Annu. Rev. Mater. Sci.* **2000**, *30*, 545−610.

(2) Matijevic, E. Production of Monodispersed Colloidal Particles. *Annu. Rev. Mater. Sci.* **1985**, *15*, 483−516.

(3) Henglein, A. Mechanism of Reactions on Colloidal Microelectrodes and Size Quantization Effects. *Top. Curr. Chem.* **1988**, *143*, 113−180.

(4) Livage, J.; Henry, M.; Sanchez, C. Sol−Gel Chemistry of Transition-Metal Oxides. *Prog. Solid State Chem.* **1988**, *18*, 259−341.

(5) Matijevic, E. Monodispersed Colloids − Art and Science. *Langmuir* **1986**, *2*, 12−20.

(6) Penn, R. L.; Stone, A. T.; Veblen, D. R. Defects and disorder: Probing the surface chemistry of heterogenite (CoOOH) by dissolution using hydroquinone and iminodiacetic acid. *J. Phys. Chem. B* **2001**, *105*, 4690−4697.

(7) Peng, X. G.; Wickham, J.; Alivisatos, A. P. Kinetics of II−VI and III−V colloidal semiconductor nanocrystal growth: "Focusing" of size distributions. *J. Am. Chem. Soc.* **1998**, *120*, 5343−5344.

(8) Rossetti, R.; Hull, R.; Gibson, J. M.; Brus, L. E. Excited Electronic States and Optical-Spectra of Zns and Cds Crystallites in the Almost-Equal-to-15 to 50-a Size Range − Evolution from Molecular to Bulk Semiconducting Properties. *J. Chem. Phys.* **1985**, *82*, 552−559.

(9) Wang, Y.; Suna, A.; Mahler, W.; Kasowski, R. Pbs in Polymers − from Molecules to Bulk Solids. *J. Chem. Phys.* **1987**, *87*, 7315−7322.

(10) Olshavsky, M. A.; Goldstein, A. N.; Alivisatos, A. P. Organometallic Synthesis of gallium-arsenide Crystallites Exhibiting Quantum Confinement. *J. Am. Chem. Soc.* **1990**, *112*, 9438−9439.

(11) Garvie, R. C. The occurrence of metastable tetragonal zirconia as a crystallite size effect. *J. Phys. Chem.* **1965**, *69*, 1238−1243.

(12) Anderson, M. A.; Gieselmann, M. J.; Xu, Q. Y. Titania and Alumina Ceramic Membranes. *J. Membr. Sci.* **1988**, *39*, 243−258.

(13) Gribb, A. A.; Banfield, J. F. Particle size effects on transformation kinetics and phase stability in nanocrystalline TiO_2. *Am. Mineral.* **1997**, *82*, 717−728.

(14) Bahnemann, D. W.; Kormann, C.; Hoffmann, M. R. Preparation and Characterization of Quantum Size Zinc-Oxide − a Detailed Spectroscopic Study. *J. Phys. Chem.* **1987**, *91*, 3789−3798.

(15) Hu, Z.; Oskam, G.; Penn, R. L.; Pesika, N.; Searson, P. C. The Influence of Anion on the Coarsening Kinetics of ZnO Nanoparticles. *J. Phys. Chem. B* **2003**, *107*, 3124−3130.

(16) Matijevic, E.; Scheiner, P. Ferric Hydrous Oxide Sols. 3. Preparation of Uniform Particles by Hydrolysis of Fe(III)-Chloride, Fe(III)-Nitrate, and Fe(III)-Perchlorate Solutions. *J. Colloid Interface Sci.* **1978**, *63*, 509−524.

(17) Leland, J. K.; Bard, A. J. Photochemistry of Colloidal Semiconducting Iron-Oxide Polymorphs. *J. Phys. Chem.* **1987**, *91*, 5076−5083.

(18) Sugimoto, T.; Matijevic, E. Formation of Uniform Spherical Magnetite Particles by Crystallization from Ferrous Hydroxide Gels. *J. Colloid Interface Sci.* **1980**, *74*, 227−243.

(19) Sampanthar, J. T.; Zeng, H. C. Arresting butterfly-like intermediate nanocrystals of ss-$Co(OH)_2$ via ethylenediamine-mediated synthesis. *J. Am. Chem. Soc.* **2002**, *124*, 6668−6675.

(20) Schwertmann, U.; Cornell, R. M. *Iron Oxides in the Laboratory: Preparation and Characterization*, 2nd ed.; Wiley-VCH: New York, 2000.

(21) Post, J. E. Manganese oxide minerals: Crystal structures and economic and environmental significance. *Proc. Natl. Acad. Sci. U.S.A.* **1999**, *96*, 3447−3454.

(22) Manceau, A.; Gorshkov, A. I.; Drits, V. A. Structural Chemistry of Mn, Fe, Co, and Ni in Manganese Hydrous Oxides. 1. Information from Xanes Spectroscopy. *Am. Mineral.* **1992**, *77*, 1133−1143.

(23) Hem, J. D.; Roberson, C. E.; Fournier, R. B. Stability of Beta Mnooh and Manganese Oxide Deposition from Springwater. *Water Resour. Res.* **1982**, *18*, 563−570.

(24) Lifshitz, I. M.; Slyozov, V. V. The kinetics of precipitation from supersaturated solid solutions. *J. Phys. Chem. Solids* **1961**, *19*, 35−50.

(25) Wagner, C. Theorie der Alterung von Niederschlägen durch Umlösen. *Z. Elektrochem.* **1961**, *65*, 581−591.

(26) Oskam, G.; Hu, Z.; Penn, R. L.; Pesika, N.; Searson, P. C. Coarsening of metal oxide nanoparticles. *Phys. Rev. E* **2002**, *66*, 011403.

(27) LaMer, V. K.; Dinegar, R. H. Theory, Prediction, and Mechanism of Formation of Monodispersed Hydrosols. *J. Am. Chem. Soc.* **1950**, *72*, 4847−4854.

(28) Huang, F.; Zhang, H. Z.; Banfield, J. F. Two-Stage Crystal-Growth Kinetics Observed during Hydrothermal Coarsening of Nanocrystalline ZnS. *Nano Lett.* **2003**, *3*, 373−378.

(29) Penn, R. L.; Banfield, J. F. Morphology development and crystal growth in nanocrystalline aggregates under hydrothermal conditions: Insights from titania. *Geochim. Cosmochim. Acta* **1999**, *63*, 1549−1557.

(30) Herrington, T. M.; Midmore, B. R. The rapid aggregation of dilute suspensions: an experimental investigation of Smoluchowski's theorem using photon correlation spectroscopy. *Powder Technol.* **1991**, *65*, 251−256.

(31) Park, J.; Privman, V. Growth of monodispersed colloids by aggregation of nucleating subunits. *Rec. Res. Dev. Stat. Phys.* **2000**, *1*, 1−17.

(32) Park, J.; Privman, V.; Matijevic, E. Model of Formation of Monodispersed Colloids. *J. Phys. Chem. B* **2001**, *105*, 11630−11635.

(33) Bitea, C.; Walther, C.; Kim, J. I.; Geckeis, H.; Rabung, T.; Scherbaum, F. J.; Cacuci, D. G. Time-resolved observation of ZrO_2-colloid agglomeration. *Colloids Surf., A* **2003**, *215*, 55−66.

(34) Libert, S.; Gorshkov, V.; Goia, D.; Matijevic, E.; Privman, V. Model of controlled synthesis of uniform colloid particles: Cadmium sulfide. *Los Alamos National Laboratory, Preprint Archive, Condensed Matter* **2003**, 1−20 (arXiv:cond-mat/0305147).

(35) Ocana, M.; Morales, M. P.; Serna, C. J. Homogeneous precipitation of uniform alpha-Fe_2O_3 particles from iron salts solutions in the presence of urea. *J. Colloid Interface Sci.* **1999**, *212*, 317−323.

(36) Ocana, M.; Morales, M. P.; Serna, C. J. The growth mechanism of alpha-Fe_2O_3 ellipsoidal particles in solution. *J. Colloid Interface Sci.* **1995**, *171*, 85−91.

(37) Shen, P.; Fahn, Y. Y.; Su, A. C. Imperfect oriented attachment: Accretion and defect generation of hexagonal inorganic-surfactant nanoparticles. *Nano Lett.* **2001**, *1*, 299−303.

(38) Penn, R. L.; Banfield, J. F. Imperfect oriented attachment: Dislocation generation in defect-free nanocrystals. *Science* **1998**, *281*, 969−971.

(39) Penn, R. L.; Banfield, J. F. Oriented attachment and growth, twinning, polytypism, and formation of metastable phases: Insights from nanocrystalline TiO_2. *Am. Mineral.* **1998**, *83*, 1077−1082.

(40) Banfield, J. F.; Welch, S. A.; Zhang, H.; Ebert, T. T.; Penn, R. L. Aggregation-based crystal growth and microstructure development in natural iron oxyhydroxide biomineralization products. *Science* **2000**, *289*, 751−754.

(41) Penn, R. L.; Banfield, J. F. Formation of rutile nuclei at anatase {112} twin interfaces and the phase transformation mechanism in nanocrystalline titania. *Am. Mineral.* **1999**, *84*, 871−876.

(42) Penn, R. L.; Oskam, G.; Strathmann, T. J.; Searson, P. C.; Stone, A. T.; Veblen, D. R. Epitaxial Assembly in Aged Colloids. *J. Phys. Chem. B* **2001**, *105*, 2177−2182.

(43) Shen, P.; Lee, W. H. (111)-specific coalescence twinning and martensitic transformation of tetragonal ZrO_2 condensates. *Nano Lett.* **2001**, *1*, 707−711.

(44) Kuo, L. Y.; Shen, P. Shape dependent coalescence and preferred orientation of CeO_2 nanocrystallites. *Mater. Sci. Eng., A* **2000**, *277*, 258−265.

(45) Zhang, H.; Banfield, J. F. New kinetic model for the nanocrystalline anatase-to-rutile transformation revealing rate dependence on number of particles. *Am. Mineral.* **1999**, *84*, 528−535.

(46) Kuo, L. Y.; Shen, P. Y. On the condensation and preferred orientation of TiC nanocrystals − effects of electric field, substrate temperature and second phase. *Mater. Sci. Eng., A* **2000**, *276*, 99−107.

(47) Banfield, J. F.; Welch, S. A.; Zhang, H. Z.; Ebert, T. T.; Penn, R. L. Aggregation-based crystal growth and microstructure development in natural iron oxyhydroxide biomineralization products. *Science* **2000**, *289*, 751−754.

(48) Banfield, J. F.; Zhang, H. Nanoparticles in the environment. *Rev. Mineral. Geochem.* **2001**, *44*, 1−58.

(49) Derjaguin, B. V.; Landau, L. *Acta Physicochim. URSS* **1941**, *14*, 633−662.

(50) Verwey, E. J.; Overbeek, J.-T. G. *Theory of the Stability of Lyophobic Colloids*; Elsevier: Amsterdam, 1948.

(51) Stokes, R. J.; Evans, D. F. *Fundamentals of Interfacial Engineering*; VCH Publishers: New York, 1997.

(52) Morel, F.-M. M.; Hering, J. G. *Principles and Applications of Aquatic Chemistry*; J. Wiley & Sons: New York, 1993.

(53) Archer, D. G.; Wang, P. The dielectric constant of water and Debye−Hueckel limiting law slopes. *J. Phys. Chem. Ref. Data* **1990**, *19*, 371−411.

(54) Burleson, D.; Penn, R. L. Two-Step Growth of Goethite from Ferrihydrite. *J. Phys. Chem. B*, in press.

(55) Sahai, N.; Sverjensky, D. A. Evaluation of internally consistent parameters for the triple-layer model by the systematic analysis of oxide surface titration data. *Geochim. Cosmochim. Acta* **1997**, *61*, 2801−2826.

(56) Hiemstra, T.; De Wit, J.-C. M.; Van Riemsdijk, W. H. Multisite proton adsorption modeling at the solid/solution interface of (hydr)oxides: a new approach, II: Application to various important (hydr)oxides. *J. Colloid Interface Sci.* **1989**, *133*, 105−117.

(57) Rustad, J. R. Proton Surface Charge Distributions on Model Goethite Nanoparticles. *Geochim. Cosmochim. Acta*, in review.

(58) Zhu, H. L.; Averback, R. S. Sintering processes of two nanoparticles: A study by molecular-dynamics. *Philos. Mag. Lett.* **1996**, *73*, 27−33.

(59) Scolan, E.; Sanchez, C. Synthesis and characterization of surface-protected nanocrystalline titania particles. *Chem. Mater.* **1998**, *10*, 3217−3223.

(60) Chemseddine, A.; Moritz, T. Nanostructuring titania: Control over nanocrystal structure, size, shape, and organization. *Eur. J. Inorg. Chem.* **1999**, 235−245.

(61) Lou, X. W.; Zeng, H. C. Complex a-MoO_3 Nanostructures with External Bonding Capacity for Self-Assembly. *J. Am. Chem. Soc.* **2003**, *125*, 2697−2704.

(62) Lee, W. H.; Shen, P. Y. On the coalescence and twinning of cube-octahedral CeO_2 condensates. *J. Cryst. Growth* **1999**, *205*, 169−176.

(63) Pacholski, C.; Kornowski, A.; Weller, H. Self-assembly of ZnO: From nanodots, to nanorods. *Angew. Chem., Int. Ed. Engl.* **2002**, *41*, 1188.

(64) Cozzoli, P. D.; Curri, M. L.; Agostiano, A.; Leo, G.; Lomascolo, M. ZnO Nanocrystals by a Non-hydrolytic Route: Synthesis and Characterization. *J. Phys. Chem. B* **2003**, in press.

(65) Niederberger, M.; Krumeich, F.; Hegetschweiler, K.; Nesper, R. An iron polyolate complex as a precursor for the controlled synthesis of monodispersed iron oxide colloids. *Chem. Mater.* **2002**, *14*, 78−82.

(66) Guyodo, Y.; Mostrom, A.; Penn, R. L.; Banerjee, S. K. From Nanodots to Nanorods: Oriented Aggregation and Magnetic Evolution of Nanocrystalline Goethite. *Geophys. Res. Lett.* **2003**, *30* (Article No. 1512).

(67) Nesterova, M.; Moreau, J.; Banfield, J. F. Model biomimetic studies of templated growth and assembly of nanocrystalline FeOOH. *Geochim. Cosmochim. Acta* **2003**, *67*, 1177−1187.

(68) Zhang, J. Z. Interfacial Charge Carrier Dynamics of Colloidal Semiconductor Nanoparticles. *J. Phys. Chem. B* **2000**, *104*, 7239−7253.

(69) Audinet, L.; Ricolleau, C.; Gandais, M.; Gacoin, T.; Boilot, J. P.; Buffat, P. A. Structural properties of coated nanoparticles: the CdS/ZnS nanostructure. *Philos. Mag. A* **1999**, *79*, 2379−2396.

(70) Ricolleau, C.; Audinet, L.; Gandais, M.; Gacoin, T. Structural transformations in II−VI semiconductor nanocrystals. *Eur. Phys. J. D* **1999**, *9*, 565−570.

(71) Nikolakis, V.; Kokkoli, E.; Tirrell, M.; Tsapatsis, M.; Vlachos, D. G. Zeolite growth by addition of subcolloidal particles: Modeling and experimental validation. *Chem. Mater.* **2000**, *12*, 845−853.

(72) de Moor, P.; Beelen, T.-P. M.; Komanschek, B. U.; Beck, L. W.; Wagner, P.; Davis, M. E.; van Santen, R. A. Imaging the assembly process of the organic-mediated synthesis of a zeolite. *Chem.—Eur. J.* **1999**, *5*, 2083−2088.

(73) Wang, Z. L. Transmission electron microscopy of shape-controlled nanocrystals and their assemblies. *J. Phys. Chem. B* **2000**, *104*, 1153−1175.